

# Triacylglycerol Accumulation Activates the Mitochondrial Apoptosis Pathway in Macrophages<sup>\*[5]</sup>

Received for publication, August 16, 2010, and in revised form, December 19, 2010. Published, JBC Papers in Press, January 1, 2011, DOI 10.1074/jbc.M110.175703

Elma Aflaki<sup>†1</sup>, Branislav Radović<sup>‡</sup>, Prakash G. Chandak<sup>‡2</sup>, Dagmar Kolb<sup>‡§</sup>, Tobias Eisenberg<sup>§</sup>, Julia Ring<sup>§</sup>, Ismene Fertschai<sup>‡</sup>, Andreas Uellen<sup>‡</sup>, Heimo Wolinski<sup>§</sup>, Sepp-Dieter Kohlwein<sup>§</sup>, Rudolf Zechner<sup>§</sup>, Sanja Levak-Frank<sup>‡</sup>, Wolfgang Sattler<sup>‡</sup>, Wolfgang F. Graier<sup>‡</sup>, Roland Malli<sup>‡</sup>, Frank Madeo<sup>§</sup>, and Dagmar Kratky<sup>‡3</sup>

From the <sup>†</sup>Institute of Molecular Biology and Biochemistry, Center of Molecular Medicine, Medical University of Graz, Harrachgasse 21, 8010 Graz, Austria and the <sup>§</sup>Institute of Molecular Biosciences, University of Graz, Heinrichstrasse 31A/Humboldtstrasse 50, 8010 Graz, Austria

Programmed cell death of lipid-laden macrophages is a prominent feature of atherosclerotic lesions and mostly ascribed to accumulation of excess intracellular cholesterol. The present *in vitro* study investigated whether intracellular triacylglycerol (TG) accumulation could activate a similar apoptotic response in macrophages. To address this question, we utilized peritoneal macrophages isolated from mice lacking adipose triglyceride lipase (ATGL), the major enzyme responsible for TG hydrolysis in multiple tissues. In *Atgl*<sup>-/-</sup> macrophages, we observed elevated levels of cytosolic Ca<sup>2+</sup> and reactive oxygen species, stimulated cytochrome *c* release, and nuclear localization of apoptosis-inducing factor. Fragmented mitochondria prior to cell death were indicative of the mitochondrial apoptosis pathway being triggered as a consequence of defective lipolysis. Other typical markers of apoptosis, such as externalization of phosphatidylserine in the plasma membrane, caspase 3 and poly-(ADP-ribose) polymerase cleavage, were increased in *Atgl*<sup>-/-</sup> macrophages. An artificial increase of cellular TG levels by incubating wild-type macrophages with very low density lipoprotein closely mimicked the apoptotic phenotype observed in *Atgl*<sup>-/-</sup> macrophages. Results obtained during the present study define a novel pathway linking intracellular TG accumulation to mitochondrial dysfunction and programmed cell death in macrophages.

in the pathogenesis of atherosclerosis. LDs are present in all eukaryotes, displaying a variable, cell- and tissue-specific composition of neutral core lipids (triacylglycerol (TG), cholesteryl esters (CE), and diacylglycerol), a phospholipid monolayer, and surface-associated proteins (1). Under hyperlipidemic conditions, macrophages incorporate modified lipoproteins and accumulate CE in LDs after esterification of unesterified “free” cholesterol (FC) by ACAT1 (acyl-CoA:cholesterol acyltransferase 1) (2). Macrophages in advanced lesions accumulate excess FC, which is a potent inducer of macrophage death (3–5). FC may be derived by hydrolysis of LD-associated CE by neutral CE hydrolases (2, 6). The origin of these enzymes and the physiological role of hormone-sensitive lipase in macrophages in this context are still matters of debate. Loading of macrophages with FC leads to caspase-dependent externalization of phosphatidylserine in the plasma membrane and to DNA fragmentation, consistent with an apoptotic process involving the Fas pathway and mitochondrial dysfunction as well as endoplasmic reticulum stress (7–11). In contrast to many studies that addressed macrophage foam cell formation in the presence of CE-containing particles, surprisingly few data have been reported on the impact of TG-rich particles in that process. Recent evidence has suggested that cholesterol and TG homeostasis may be functionally linked because increased TG concentrations within lysosomes induced the removal of cholesterol, thus stimulating cholesterol efflux from the foam cell (12).

Excessive lipid storage in lipid droplets (LDs)<sup>4</sup> of macrophage-derived foam cells is an early and possibly decisive event

Both fatty acids and FC are mobilized from neutral lipid stores by intracellular lipases. Adipose triglyceride lipase (ATGL) catalyzes the initial step of TG hydrolysis in most tissues, generating diacylglycerol and free fatty acids (FFAs) (13–15). Hormone-sensitive lipase was reported to be more effective in hydrolyzing diacylglycerol compared with TG (16). ATGL deficiency in mice results in increased fat mass due to an 80% reduction in TG hydrolase activity and a concomitant TG accumulation in cardiomyocytes leading to heart failure and premature death (17). Similarly, a mutation in the human ATGL gene was found to cause neutral lipid storage disease with myopathy (18); notably, the same mutation was observed in a patient who underwent cardiac transplantation because of cardiomyopathy

<sup>\*</sup> This work was supported by the Medical University of Graz (Ph.D. Program “Molecular Medicine”), the Austrian Science Fund FWF (SFB-LIPOTOX F30 and P19186), and the Austrian Federal Ministry of Science and Research (GEN-AU project Genomics of Lipid-associated Disorders).

<sup>[5]</sup> The on-line version of this article (available at <http://www.jbc.org>) contains supplemental Figs. S1–S6.

⌘ Author's Choice—Final version full access.

<sup>1</sup> Supported by the Medical University of Graz Ph.D. Program in Molecular Medicine.

<sup>2</sup> Fellow of the Medical University of Graz Ph.D. Program in Molecular Medicine.

<sup>3</sup> To whom correspondence should be addressed. Tel.: 43-316-380-7543; Fax: 43-316-380-9615; E-mail: dagmar.kratky@medunigraz.at.

<sup>4</sup> The abbreviations used are: LD, lipid droplet; TG, triacylglycerol; CE, cholesteryl ester(s); FC, free cholesterol; ATGL, adipose triglyceride lipase; FFA, free fatty acid; acLDL, acetylated LDL; LPDS, lipoprotein-deficient serum; HPRT, hypoxanthine-guanine phosphoribosyltransferase; PI, propidium iodide; AIF, apoptosis-inducing factor; BHQ, 2,5-di-*t*-butyl-1,4-benzohydroquinone; SERCA, sarcoplasmic/endoplasmic reticulum Ca<sup>2+</sup>; DCFDA, 5-(and-6)-chloromethyl-2',7'-dichlorodihydrofluorescein diacetate, acetyl

ester; DCF, 2',7'-dichlorodihydrofluorescein; FCCP, carbonyl cyanide *p*-(trifluoromethoxy)phenylhydrazone; PARP, poly(ADP-ribose) polymerase; ROS, reactive oxygen species; ANOVA, analysis of variance.

(19). Since then, several other mutations in the ATGL gene locus have been discovered in patients (20, 21).

We have shown recently that murine *Atgl*<sup>-/-</sup> macrophages accumulate high amounts of TG-rich LD (22), and this allowed us to explore the consequences of increased intracellular TG concentrations on macrophage viability and cell death. The present data suggest that TG accumulation in untreated *Atgl*<sup>-/-</sup> macrophages results in spontaneous programmed cell death. We compared these results with macrophages incubated with acetylated low density lipoprotein (acLDL) and the ACAT inhibitor 58035 as a positive control of an apoptotic cell model induced by elevated levels of FC. Similar to *Atgl*<sup>-/-</sup> macrophages, TG accumulation in wild-type (WT) macrophages exogenously loaded with very low density lipoprotein (VLDL) macrophages triggers programmed cell death involving mitochondrial dysfunction and activation of the mitochondrial apoptosis pathway. Our findings provide novel insight into lipotoxic effects of TG accumulation in macrophages. The work extends our recognition of the fundamental significance of maintaining TG homeostasis and downstream processes involved in generating lipid-derived apoptotic signals.

## EXPERIMENTAL PROCEDURES

**Animals**—*Atgl*<sup>-/-</sup> mice were generated as described elsewhere (17). All studies were performed with *Atgl*<sup>-/-</sup> mice and WT littermates backcrossed at least seven times on a C57Bl/6 genetic background. The mice were kept on a standard chow diet (4% fat and 21% protein; ssniff, Soest, Germany) on a regular 12-h dark/light cycle. Animal experiments were performed in accordance with the standards established by the Austrian Federal Ministry of Science and Research, Division of Genetic Engineering and Animal Experiments (Vienna, Austria).

**Cell Culture**—Macrophages were harvested from the peritoneum of 7–8-week-old female *Atgl*<sup>-/-</sup> and WT mice 3 days after intraperitoneal injection of 3 ml of 3% thioglycolate medium. Cells were washed three times with PBS and cultivated in Dulbecco's modified Eagle's medium (DMEM), 10% lipoprotein-deficient serum (LPDS), and 100 µg/ml penicillin/streptomycin. As a positive control for cells that undergo apoptosis, we incubated macrophages with 100 µg/ml acLDL for 24 h plus ACAT inhibitor 58035 (10 µg/ml; Sandoz, Kundl, Austria) for the last 12 h (FC-loaded macrophages) (7, 8). To achieve intracellular TG accumulation in WT macrophages, we incubated the cells with 150 µg of VLDL/ml for 24 h (VLDL-loaded WT cells). LDL and VLDL were isolated from human plasma by density gradient ultracentrifugation. LDL was acetylated as described (23).

**Macrophage Lipid Parameters**—Lipids were extracted from cells with 2 ml of hexane/isopropyl alcohol (3:2, v/v) for 1 h at 4 °C. Lipid extracts were dried under nitrogen, redissolved in 100 µl of 1% Triton X-100 in chloroform, dried under nitrogen, and resuspended in 100 µl of distilled water for 15 min at 37 °C. Aliquots (30 µl) were used for enzymatic measurements of TG (Diagnostic Systems, Holzheim, Germany), TC (Greiner Diagnostics AG, Bahlingen, Germany), and FC (Diagnostic Systems, Holzheim, Germany) concentrations. Protein was quantified using a Bradford assay (Bio-Rad) after dissolving the proteins

from extracted cells in 2 ml of 0.3 M NaOH for 1 h at room temperature, using bovine serum albumin as a standard.

**FFA Analysis**—For the preparation of pentafluorobenzyl-ester derivatives, cellular lipids were extracted twice in hexane/isopropyl alcohol (3:2, v/v) in the presence of 2.5 µg of stearic-*d*<sub>35</sub> acid (C18:0-*d*<sub>35</sub>, Isotec) as internal standard. One hundred µl of 1-ml lipid extract were converted to the corresponding pentafluorobenzyl-ester derivatives in 50 µl of acetonitrile containing 2% (v/v) pentafluorobenzyl bromide (Sigma-Aldrich) and 2% (v/v) *N,N*-diisopropylethylamine (Sigma-Aldrich). After 30 min at 25 °C samples were dried under vacuum, redissolved in 100 µl of hexane, transferred to autosampler vials, and stored at -20 °C. For GC-MS analysis, a Thermo Scientific Trace GC coupled to a DSQII mass spectrometer was used. The GC was fitted with a SGE BPX5 capillary column (30 meters, 0.25-mm inner diameter, 0.25-µm methyl silicone film coating). The injector was operated in the splitless mode at 230 °C. Helium was used as carrier gas at a flow rate of 1.5 ml/min. Initial column temperature was 120 °C for 2 min, followed by an increase of 20 °C/min to 160 °C, an isothermal hold of 2 min, a second increase at 12 °C/min to 300 °C, an isothermal hold for 2 min, and an increase by 10 °C/min to 320 °C with a hold for 2 min. The transfer line was kept at 300 °C, and the ion source was 225 °C. Negative ion chemical ionization was performed with an electron energy of 70 eV and an emission current of 100 µA. Methane (2.5 ml/min) was used as reagent gas. Quantitation was performed by peak area comparison along with a standard calibration curve consisting of unlabeled primary fatty acid standards (Sigma-Aldrich) mixed with the stable isotope-labeled standard.

**Real-time PCR**—Total RNA was isolated from control and FC- and VLDL-loaded macrophages from *Atgl*<sup>-/-</sup> and WT mice using the peqGOLD kit (PeqLab, Vienna, Austria) according to the manufacturer's instructions. Two µg of total RNA were reverse transcribed using the High Capacity cDNA Reverse Transcription Kit (Applied Biosystems, Vienna, Austria). Quantitative real-time PCR was performed on an ABI prism 7900 real-time PCR instrument (Applied Biosystems, Vienna, Austria) using the Quantifast SYBR Green PCR kit (Qiagen, Hilden, Germany). Primer sequences are available upon request. Data are displayed as expression ratios of target genes normalized to the expression of hypoxanthine-guanine phosphoribosyltransferase (HPRT) as an internal reference in each sample.

**Apoptosis Assay**—Apoptosis in macrophages and FC- and VLDL-loaded cells was assayed by annexin V and propidium iodide (PI) co-staining using an Annexin-V-FLUOS staining kit (Roche Applied Science). After incubation, the cells were gently washed once with PBS and incubated for 15 min at room temperature with 120 µl of annexin-binding buffer (25 mmol/liter HEPES, 140 mM NaCl, 1 mM EDTA, pH 7.4, 0.1% BSA) containing 10 µl of FITC-conjugated annexin V and 1 µl of PI (100 µg/ml). The staining mixture was then removed and replaced with 120 µl of annexin-binding buffer. The cells were immediately viewed at room temperature by fluorescence microscopy (Zeiss Axioskop; Carl Zeiss GmbH, Vienna, Austria) equipped with a 10× objective and filters appropriate for fluorescein (annexin V) and rhodamine (PI). For quantification, three fields

## Macrophage Apoptosis by Intracellular TG Accumulation

of cells (~700 cells/field) for each condition were counted. The number of annexin V/PI-positive cells in each field is expressed as the percentage of these cells per total cells counted.

**Isolation of Cytosolic Fractions**—Mitochondria- and nucleus-free cytosolic fractions were isolated from untreated and FC- and VLDL-loaded macrophages using the Benchtop mitochondria isolation kit (Mitoscience, Eugene, OR) according to the manufacturer's instructions. Cytosolic fractions were subjected to electrophoresis and assayed for Bax, Bcl-2, and cytochrome *c* by Western blotting.

**Western Blotting Analysis**—Untreated and FC- and VLDL-loaded macrophages were washed twice with PBS and lysed in radioimmune precipitation assay buffer (50 mM Tris/HCl, pH 8, 150 mM NaCl, 1% Triton X-100, and 50% sodium deoxycholate) in the presence of 1  $\mu$ g of protease inhibitor mixture (Sigma-Aldrich). Forty  $\mu$ g of proteins were separated on a 12.5% SDS-polyacrylamide gel by electrophoresis and electroblotted onto nitrocellulose Protran BA85 membranes (Whatman, Vienna, Austria). The blots were blocked in 5% BSA plus 0.1% Tween 20 and incubated with the following primary polyclonal antibodies (if not stated otherwise): anti-rabbit cytochrome *c* (1:100), anti-rabbit Bax (1:500), anti-rabbit poly(ADP-ribose) polymerase (PARP) (1:800), and anti-rabbit Bcl-2 (1:500) (all purchased from Cell Signaling, Vienna, Austria) and anti-rabbit caspase 3 (1:50) and monoclonal anti-mouse  $\beta$ -actin (1:1000) (both purchased from Santa Cruz Biotechnology, Heidelberg, Germany). All blots were incubated overnight at 4 °C. The horseradish peroxidase-conjugated goat anti-rabbit (1:5000) (Santa Cruz Biotechnology) and rabbit anti-mouse antibodies (1:1000) (Dako, Glostrup, Denmark) were visualized by enhanced chemiluminescence detection (ECL Plus, Amersham Biosciences) on an AGFA Curix Ultra X-Ray film (Siemens, Graz, Austria).

**Immunofluorescence of Apoptosis-inducing Factor (AIF)**—WT and *Atgl*<sup>-/-</sup> macrophages were fixed with 4% formaldehyde in PBS for 30 min at room temperature. Cells were permeabilized with 0.5% Triton X-100 in 3% skim milk for 60 min. Thereafter, cells were incubated with anti-AIF (1:300) (Cell Signaling) for 1 h. The cells were stained for 1 h with anti-rabbit AlexaFluor-594 (1:250) (Molecular Probes, Invitrogen) for visualization of AIF. After washing the cells with PBS, they were mounted in Vectashield/DAPI (Vector, Burlingame, CA). Images were taken on an Olympus FSX100 fluorescence microscope (Olympus, Hamburg, Germany).

**Caspase 3/7 Activity Assay**—Macrophages from WT and *Atgl*<sup>-/-</sup> mice were cultivated in DMEM, 10% LPDS. The combined caspase 3 and 7 activities were measured using the Caspase-GLO<sup>®</sup>3/7 assay (Promega, Vienna, Austria) according to the manufacturer's instructions. Luminescence was determined on a TopCount NXT luminometer (Packard Instruments, Meriden, CT).

**Mitochondria and Lipid Droplet Staining**—Mitochondria of untreated and FC- and VLDL-loaded macrophages were stained using 0.5  $\mu$ M MitoTracker Green (Molecular Probes, Invitrogen) (37 °C, 5 min). LDs were visualized by Nile Red (2.5  $\mu$ g/ml) staining. Z-stacks were recorded using a Leica SP5 AOBs confocal microscope (Leica Microsystems, Vienna, Austria).

**Electron Microscopy**—Macrophages grown on a Melinex film (Gröpl, Tulln, Austria) were fixed in 0.06 M phosphate buffer (pH 7.2) containing 2.5% glutaraldehyde for 90 min at room temperature. Macrophages were rinsed twice in 0.06 M phosphate buffer for 10 min and postfixed in 1% osmium tetroxide in the same buffer for 1 h. Cells were rinsed four times for 10 min in 0.06 M phosphate buffer and dehydrated in a series of 50, 70, 90, and 100% cold acetone, for 20 min each. Cells were infiltrated by 2:1, 1:1, and 1:2 mixtures of 100% acetone and agar 100 epoxy resin (Gröpl) and pure agar 100 epoxy resin for 4 h. Finally, cells were placed in agar 100 epoxy resin at room temperature for 8 h, transferred into embedding molds, and polymerized at 60 °C for 48 h. Ultrathin sections (75 nm) were cut with a Reichert Ultracut S Ultramicrotome and stained with lead citrate for 5 min and with uranyl acetate for 15 min. Images were taken on a Zeiss EM 902 transmission electron microscope equipped with a ProScan slow scan CCD camera.

**Cytosolic Ca<sup>2+</sup> Measurements**—Cells grown on coverslips in 6-well dishes were loaded with 4  $\mu$ M fura-2 (Molecular Probes) and sulfinpyrazone (250  $\mu$ M) (Sigma-Aldrich) at room temperature for 30 min as described previously (10). After 100 s, 15  $\mu$ M SERCA inhibitor 2,5-di-*t*-butyl-1,4-benzohydroquinone (BHQ) was added to empty endoplasmic Ca<sup>2+</sup> pools into the cytosol. Fluorescence images (510-nm emission after alternate 340- and 380-nm excitation) of ~300 cells were collected by fluorescence microscopy. Each image was corrected for background fluorescence, and the 340:380 nm fluorescence ratio of individual cells was calculated.

**Intracellular Reactive Oxygen Species (ROS) Measurements**—WT and *Atgl*<sup>-/-</sup> macrophages were incubated with 5-(and-6)-chloromethyl-2',7'-dichlorodihydrofluorescein diacetate, acetyl ester (DCFDA, 50  $\mu$ M) (Sigma-Aldrich) for 10 min. Intracellular ROS production in macrophages was determined by the hydrolysis of DCFDA to fluorescent 2',7'-dichlorofluorescein and internalization, which is generally exerted by several reactive radical species and allows the assessment of general oxidative stress (24). DCFDA conversion was measured in a FlexStation<sup>™</sup> II device (Molecular Devices, Downingtown, PA) (excitation, 488 nm; emission, 535 nm).

**Oxygen Consumption**—Macrophages from WT and *Atgl*<sup>-/-</sup> mice cultivated in DMEM, 10% LPDS were analyzed by intact cell respirometry in different states of mitochondrial respiration *in situ* by using an Oxygraph-2k respirometer (Oroboros Instruments, Innsbruck, Austria). Basal cellular O<sub>2</sub> consumption was recorded without metabolic inhibitors or uncouplers. ATP synthase was inhibited with 2  $\mu$ g/ml oligomycin, followed by uncoupling of the respiratory chain from oxidative phosphorylation by stepwise titration with carbonyl cyanide *p*-(trifluoromethoxy)phenylhydrazone (FCCP) to achieve maximal O<sub>2</sub> consumption. Oxygen consumption rates were normalized to basal values obtained by inhibiting mitochondrial O<sub>2</sub> consumption by the addition of 1 M KCN to inhibit cytochrome *c* oxidase.

**Statistics**—Statistical analyses were performed using GraphPad Prism 5.0 software. The significance was determined by Student's *t* test. Data with >2 groups or  $\geq 2$  independent variables were analyzed by ANOVA, followed by the Bonferroni *post hoc* test. Data are presented as mean values  $\pm$  S.E. Significance levels between WT and *Atgl*<sup>-/-</sup> macrophages or

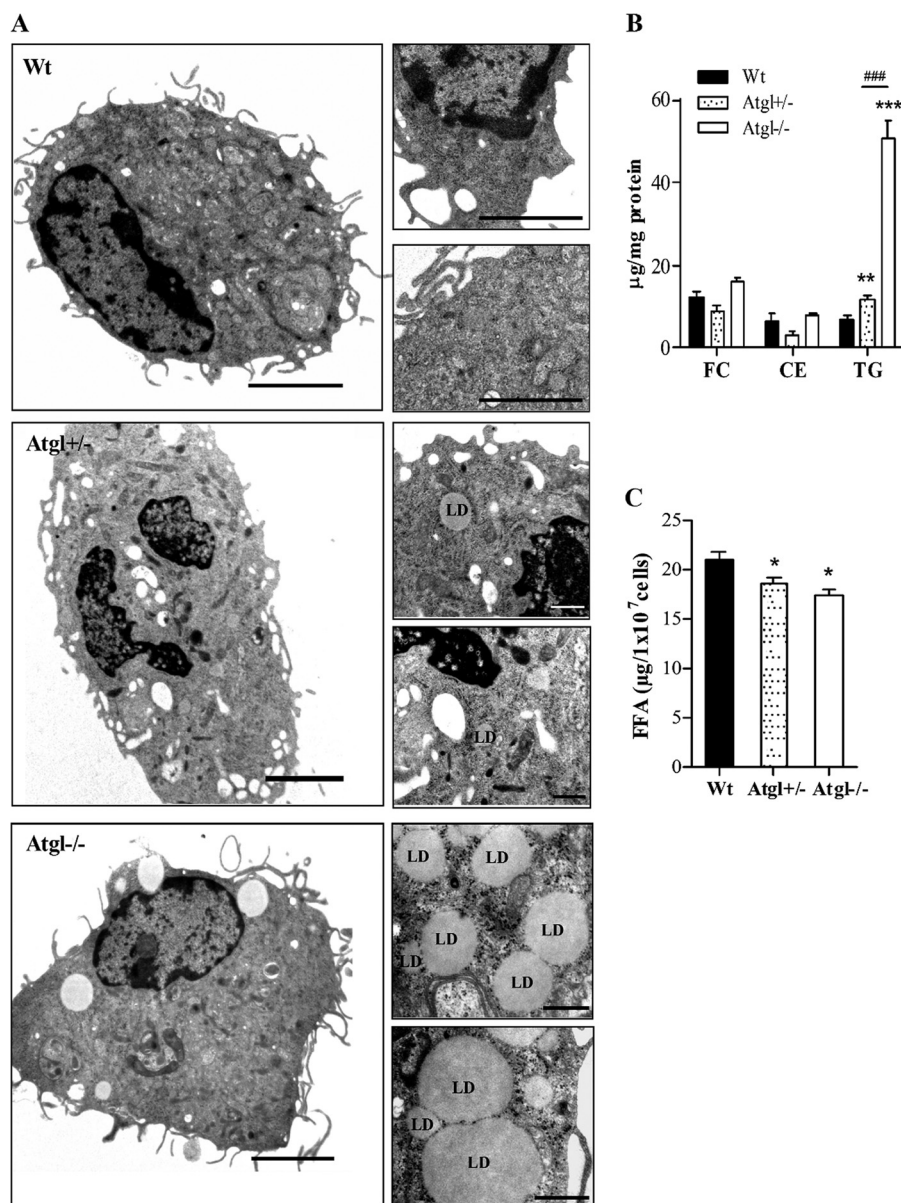


**FIGURE 1. Lipid droplet accumulation in *Atgl*<sup>-/-</sup> macrophages.** *A*, representative electron micrographs of WT, *Atgl*<sup>+/-</sup>, and *Atgl*<sup>-/-</sup> peritoneal macrophages showing LDs in *Atgl*<sup>-/-</sup> macrophages. Scale bars, 2  $\mu$ m (whole cell) and 0.5  $\mu$ m (sections). *B*, lipid parameters in macrophages from WT, *Atgl*<sup>+/-</sup>, and *Atgl*<sup>-/-</sup> mice. Data are mean values ( $n = 3-6$ )  $\pm$  S.E. (error bars) of experiments performed in duplicate. *C*, total FFA concentrations (sum of C14:0, C16:0, C16:1, C18:0, C18:1, C18:2, C20:4, and C22:6) are presented as means ( $n = 3-4$ )  $\pm$  S.E. \*,  $p < 0.05$ ; \*\*,  $p \leq 0.01$ ; \*\*\*,  $p \leq 0.001$ ; ###,  $p \leq 0.001$  by ANOVA followed by Bonferroni's *post hoc* test.

untreated and VLDL-loaded WT cells were set at  $p < 0.05$  (\*),  $p \leq 0.01$  (\*\*),  $p \leq 0.001$  (\*\*\*) and  $p < 0.05$  (#),  $p \leq 0.01$  (##),  $p \leq 0.001$  (###) between different conditions.

## RESULTS

*Atgl*<sup>-/-</sup> Macrophages Display Hallmark Features of Apoptosis—Peritoneal macrophages isolated from WT, *Atgl*<sup>+/-</sup> and *Atgl*<sup>-/-</sup> mice were investigated by electron microscopy to monitor LD accumulation. Whereas WT and *Atgl*<sup>+/-</sup> macrophages lack numerous lipid inclusions, *Atgl*<sup>-/-</sup> macrophages accumulate LD even in the absence of exogenous lipid loading (Fig. 1*A*). TG concentrations were elevated 1.7-fold in *Atgl*<sup>+/-</sup> compared with WT macrophages, whereas *Atgl*<sup>-/-</sup> macrophages exhibited a 7.2-fold increase in intracellular TG levels

compared with WT macrophages (Fig. 1*B*). FC and CE levels were comparable between macrophages from all genotypes. FFA concentrations in freshly isolated macrophages without any exogenous stimulus were slightly but significantly reduced in *Atgl*<sup>-/-</sup> and *Atgl*<sup>+/-</sup> compared with WT macrophages (Fig. 1*C*).

To investigate the impact of ATGL on cell viability, we analyzed various markers of apoptotic and necrotic cell death in *Atgl*<sup>-/-</sup> and *Atgl*<sup>+/-</sup> macrophages. WT macrophages loaded with acLDL in the presence of the ACAT inhibitor 58035 (FC-loaded) were used as a positive control for cells that undergo apoptosis (7, 8, 10). To monitor macrophage cell death, we compared annexin V and PI co-staining in macrophages isolated from *Atgl*<sup>-/-</sup>, *Atgl*<sup>+/-</sup>, and WT mice (Fig. 2*A*). Quantifi-

## Macrophage Apoptosis by Intracellular TG Accumulation

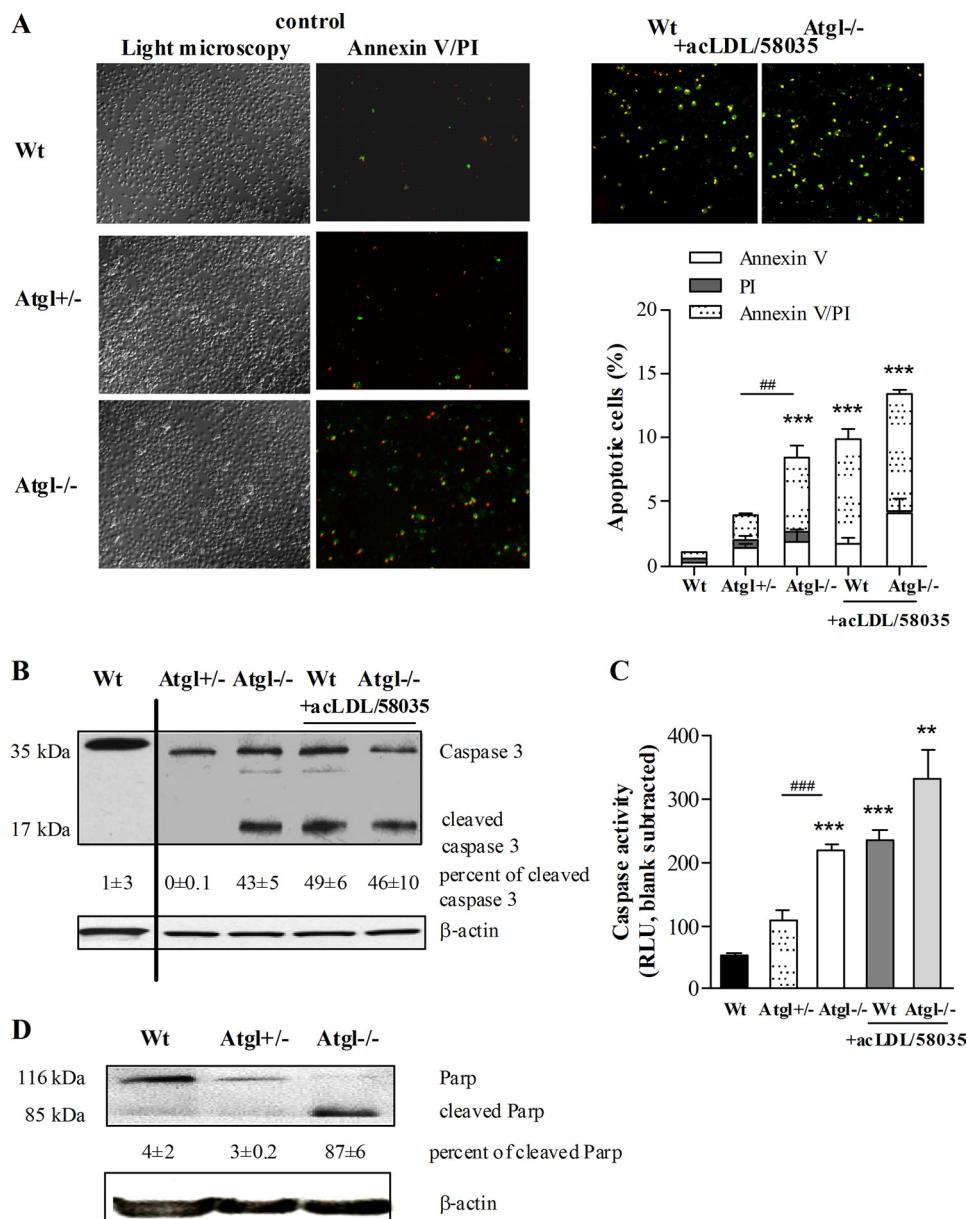


**FIGURE 2. Induction of apoptosis in *Atgl*<sup>-/-</sup> macrophages.** *A*, macrophages were isolated from three WT, *Atgl*<sup>+/-</sup>, and *Atgl*<sup>-/-</sup> mice and cultivated in DMEM, 10% LPDS or treated for 24 h with acLDL (100  $\mu$ g/ml) in the presence of the ACAT inhibitor 58035 (10  $\mu$ g/ml) for the last 12 h, resembling FC loading. Apoptosis was assessed after co-staining with FITC-conjugated annexin V (green) and PI (red), respectively, by fluorescence microscopy. Original magnification,  $\times 10$ . Seven fields of cells with  $\sim 700$  cells/field were counted for each condition. Data are expressed as the percentage of total cells that stained with annexin V and PI. Quantifications of the total amount of annexin V/PI-positive, annexin V-positive, and PI-positive cells are shown as means  $\pm$  S.E. (error bars) of four independent experiments performed in duplicate. \*\*\*,  $p \leq 0.001$ ; ##,  $p \leq 0.01$  by ANOVA followed by Bonferroni's *post hoc* test. *B* and *D*, cell lysates of WT, *Atgl*<sup>+/-</sup>, and *Atgl*<sup>-/-</sup> mice (40  $\mu$ g of protein/lane) were separated by SDS-PAGE. Protein levels of cleaved caspase 3 (*B*) and PARP (*D*) were analyzed by Western blotting experiments. Abundance of the cleaved proteins was quantified relative to the uncleaved proteins. Data are presented as means of 2–3 independent experiments  $\pm$  S.E. *C*, combined caspase 3 and 7 activities were measured in cell lysates from WT, *Atgl*<sup>+/-</sup>, and *Atgl*<sup>-/-</sup> macrophages and FC-loaded cells. Data are presented as mean values ( $n = 4$ )  $\pm$  S.E. \*\*\*,  $p \leq 0.001$ ; ###,  $p \leq 0.001$  by ANOVA followed by Bonferroni's *post hoc* test. RLU, relative luminescence units.

cation of the annexin V/PI co-stainings revealed that only 1% of WT cells exhibited externalization of phosphatidylserine (annexin V-positive), indicative of cells undergoing apoptosis, under the experimental conditions used (Fig. 2A). *Atgl*<sup>+/-</sup> macrophages showed 3.5-fold more annexin V-positive cells; however, this increase lacked statistical significance. In contrast, the 8-fold increased number of annexin V-positive cells in the population of *Atgl*<sup>-/-</sup> macrophages indicated higher susceptibility of these cells to apoptosis. *Atgl*<sup>+/-</sup> macrophages showed an increased percentage of apoptotic cells compared

with WT macrophages; however, this elevation lacked statistical significance. In all macrophages, we considered both annexin V single positives (early apoptotic cells) and annexin V/PI double positives (late apoptotic cells) as cells that died primarily from apoptosis. To verify this interpretation, we treated macrophages with high peroxide concentrations to induce necrotic cell death and tested for “non-apoptotic” binding of annexin V under necrotic conditions. These cells showed efficient staining by PI but lacked any staining by annexin V (data not shown). Incubation of WT macrophages with FC

resulted in elevated levels of annexin V/PI staining, showing a similar induction of apoptosis as observed in unloaded *Atgl*<sup>-/-</sup> macrophages (Fig. 2A). Additional stress by loading with FC does not significantly increase apoptosis in *Atgl*<sup>-/-</sup> macrophages. These findings suggest that programmed cell death in TG-rich *Atgl*<sup>-/-</sup> macrophages is triggered spontaneously without any further exogenous treatment.

Next, we performed immunoblotting to test for cleavage of caspase 3 and PARP, two other markers of apoptosis. Whereas cleavage of caspase 3 was not detectable in WT and *Atgl*<sup>+/-</sup> macrophages, incubation of WT macrophages with FC resulted in caspase 3 cleavage (Fig. 2B). In contrast, caspase 3 cleavage was observed in unloaded *Atgl*<sup>-/-</sup> macrophages. Consistently, the combined caspase 3 and 7 activities were 4.2-fold increased in untreated *Atgl*<sup>-/-</sup> macrophages compared with the WT controls (Fig. 2C). No significant increase in caspase 3/7 activity was observed in *Atgl*<sup>+/-</sup> macrophages. Loading of WT and *Atgl*<sup>-/-</sup> macrophages with FC resulted in similarly elevated levels of cleaved caspase 3 as observed in untreated *Atgl*<sup>-/-</sup> macrophages, indicating that the FC loading in *Atgl*<sup>-/-</sup> cells does not further stimulate caspase 3 processing. Moreover, the majority of cellular PARP was present in the cleaved form in *Atgl*<sup>-/-</sup> macrophages (87%), which was largely absent in WT and *Atgl*<sup>+/-</sup> macrophages (4 and 3%, respectively) (Fig. 2D). Based on the analysis of apoptotic markers, it is evident that macrophages derived from *Atgl*<sup>-/-</sup> mice show increased susceptibility to apoptotic cell death.

**Mitochondrial Dysfunction in *Atgl*<sup>-/-</sup> Macrophages**—The apoptotic phenotypes described above prompted us to investigate the expression of typical apoptotic executors and inhibitors in *Atgl*<sup>-/-</sup> macrophages. Anti-apoptotic Bcl-XL mRNA was reduced by 91% in *Atgl*<sup>-/-</sup> compared with WT macrophages, and the level of Mcl-1 mRNA was decreased by 57% (Fig. 3A). *Atgl*<sup>+/-</sup> macrophages showed 25–27% reduced mRNA levels of Bcl-XL and Mcl-1. The protein expression of Bcl-2 was slightly reduced in *Atgl*<sup>+/-</sup> macrophages and decreased by 59% in *Atgl*<sup>-/-</sup> compared with WT macrophages (Fig. 3B). We failed to detect any differences in Bax protein expression between *Atgl*<sup>+/-</sup> and WT but observed a more than 3-fold increase in *Atgl*<sup>-/-</sup> macrophages. Because Bax is proposed to induce the opening of the outer mitochondrial membrane channels, resulting in the release of proapoptotic factors, we determined mitochondrial cytochrome *c* release into the cytosol. WT macrophages lacked any cytosolic cytochrome *c* expression. In contrast, cytochrome *c* was slightly increased in *Atgl*<sup>+/-</sup> compared with WT macrophages and readily detectable in the cytosol from untreated *Atgl*<sup>-/-</sup> macrophages. Exogenous triggering of apoptosis by FC loading resulted in reduced Bcl-2 and increased Bax protein expression and cytochrome *c* release in both genotypes, which were comparable with the expression levels observed in untreated *Atgl*<sup>-/-</sup> macrophages (Fig. 3B).

Loading of macrophages with FC is associated with mitochondrial dysfunction and activation of the mitochondrial apoptosis pathway (8). Therefore, we next performed a JC-1 assay to determine the mitochondrial membrane potential ( $\Delta\Psi_m$ ) of *Atgl*<sup>-/-</sup> macrophages. We observed a  $16 \pm 1\%$  decrease in the JC-1 red/green fluorescence ratio in *Atgl*<sup>-/-</sup> compared with

WT macrophages, suggesting a decrease in the  $\Delta\Psi_m$ . Fluorescence and electron microscopy revealed that mitochondria in WT and *Atgl*<sup>+/-</sup> macrophages showed an intact ultrastructure with unfragmented mitochondria (Fig. 3C and supplemental Figs. S1 and S2). Mitochondria of *Atgl*<sup>-/-</sup> macrophages, however, were substantially fragmented (Fig. 3C and supplemental Fig. S3), which is a defining feature of apoptosis. Additionally, the size of mitochondria in *Atgl*<sup>-/-</sup> macrophages ( $0.37 \pm 0.16 \mu\text{m}$ ) was drastically reduced compared with *Atgl*<sup>+/-</sup> ( $0.58 \pm 0.24 \mu\text{m}$ ) and WT mitochondria ( $0.71 \pm 0.28 \mu\text{m}$ ) (supplemental Fig. S4). Several mitochondria in *Atgl*<sup>-/-</sup> macrophages have less or no cristae, providing further evidence for considerable mitochondrial dysfunction in these cells.

To obtain further insight into the molecular basis for mitochondrial dysfunction in *Atgl*<sup>-/-</sup> macrophages, we determined mRNA levels of genes important in the mitochondrial electron transport system. The mRNA level of NADH:ubiquinone oxidoreductase (complex I) was reduced by 87% in *Atgl*<sup>-/-</sup> macrophages and NADPH oxidase activator (Noxa1), which triggers the generation of O<sub>2</sub><sup>-</sup>, was increased 4.8-fold (Fig. 3D). We failed to detect significant changes in the mRNA levels of complex I and Noxa1 in *Atgl*<sup>+/-</sup> macrophages. Intracellular ROS production, as monitored by the conversion of DCFDA to fluorescent DCF, was 9.6-fold higher in *Atgl*<sup>-/-</sup> compared with WT macrophages (Fig. 3E). We also observed increased ROS production in *Atgl*<sup>+/-</sup> macrophages; however, this increase lacked significance.

Deficiency of ATGL was also accompanied by significantly reduced mitochondrial O<sub>2</sub> consumption. Measurement of basal respiration demonstrated that *Atgl*<sup>-/-</sup> macrophages consumed O<sub>2</sub> at a 65% reduced rate compared with WT macrophages (Fig. 3F). This difference was mainly due to a strong reduction in the oligomycin-sensitive respiration (*i.e.* oxidative phosphorylation). The maximal O<sub>2</sub> consumption, determined by uncoupling the respiratory chain with FCCP, was reduced by 70% in *Atgl*<sup>-/-</sup> compared with WT macrophages. Accordingly, the spare respiratory capacity, which is calculated as the difference between the mitochondrial O<sub>2</sub> consumption under basal conditions and the maximal O<sub>2</sub> consumption, was reduced by 73% in *Atgl*<sup>-/-</sup> compared with WT macrophages (Fig. 3F).

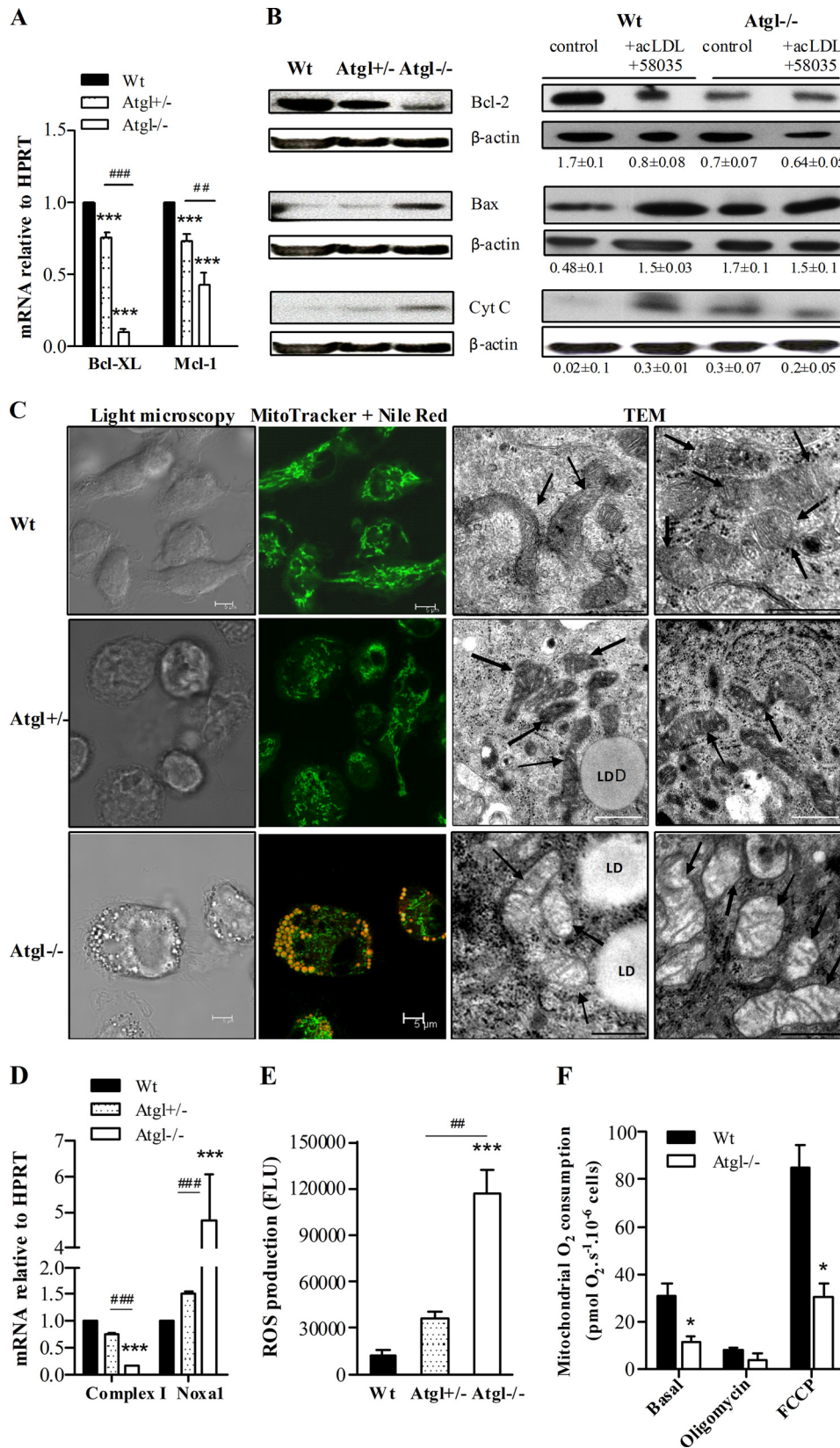
When we incubated the macrophages with fura-2, we observed a clear increase of the basal  $F_{340}/F_{380}$  ratio in *Atgl*<sup>-/-</sup> compared with WT macrophages, indicating that the cytosolic Ca<sup>2+</sup> concentration ( $[\text{Ca}^{2+}]_{\text{cyto}}$ ) is significantly elevated in cells lacking ATGL (Fig. 4A). To test whether or not the endoplasmic reticulum Ca<sup>2+</sup> content is affected in *Atgl*<sup>-/-</sup> macrophages,  $[\text{Ca}^{2+}]_{\text{cyto}}$  signals were recorded upon SERCA inhibition with BHQ in the absence of extracellular Ca<sup>2+</sup>. This yields an elevation of  $[\text{Ca}^{2+}]_{\text{cyto}}$  due to a passive Ca<sup>2+</sup> leak from the endoplasmic reticulum. As shown in Fig. 4, A and B, *Atgl*<sup>-/-</sup> macrophages displayed a markedly reduced response to BHQ compared with WT cells, suggesting that the endoplasmic reticulum Ca<sup>2+</sup> content was decreased in *Atgl*<sup>-/-</sup> macrophages. Increasing the intracellular Ca<sup>2+</sup> levels is a prerequisite for processing and release of AIF. Indeed, we observed a nuclear localization of AIF in *Atgl*<sup>-/-</sup> macrophages, which is generally associated with apoptosis (Fig. 4C).

## Macrophage Apoptosis by Intracellular TG Accumulation

Taken together, these data clearly demonstrate a highly compromised mitochondrial function as a consequence of defective lipolysis, resulting in mitochondrial fragmentation, loss of membrane potential, reduced oxygen

consumption, and elevated cytosolic  $Ca^{2+}$  levels and ROS production.

*VLDL Loading Increases Apoptosis in WT Macrophages—* Mitochondrial dysfunction and apoptosis in *Atgl*<sup>-/-</sup> macro-



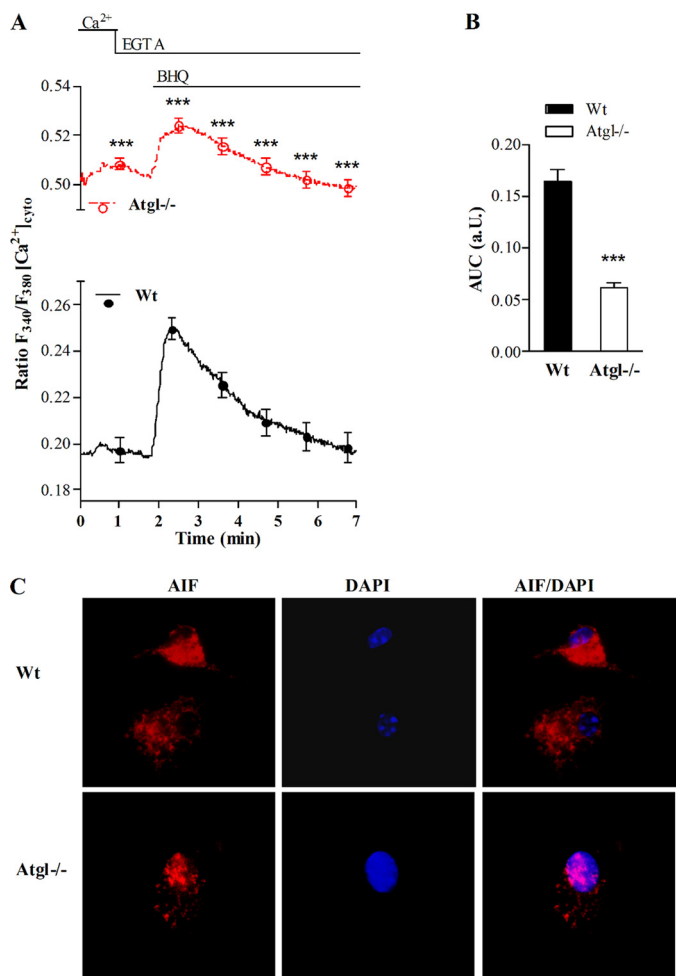


**FIGURE 4. Elevation of cytosolic  $\text{Ca}^{2+}$  and nuclear localization of AIF in  $\text{Atgl}^{-/-}$  macrophages.** WT and  $\text{Atgl}^{-/-}$  macrophages were plated on coverslips in DMEM, 10% LPDS. A, the fura-2 fluorescence ratio (340/380 nm) was determined in single macrophages before and after the addition of BHQ (15 mM). Data are expressed as mean values of  $\sim 300$  cells/genotype of three independent experiments  $\pm$  S.E. B, the area under the curve was calculated after the addition of BHQ in WT and  $\text{Atgl}^{-/-}$  macrophages. Data are presented as means  $\pm$  S.E. \*\*\*,  $p \leq 0.001$  determined by Student's  $t$  test. C, WT and  $\text{Atgl}^{-/-}$  macrophages were fixed and incubated with anti-AIF antibody for 1 h. To visualize AIF, cells were then incubated with anti-rabbit AlexaFluor-594 and mounted in Vectashield/DAPI to visualize the nucleus. Representative images taken by fluorescence microscopy are shown.

phages may be due to increased levels of TG or reduced lipolysis and release of FFAs as substrates of  $\beta$ -oxidation. To discriminate between these possibilities, we examined whether VLDL-induced TG loading of macrophages can phenocopy the conse-

quences of genetically induced TG accumulation by ATGL deficiency. Therefore, we incubated WT macrophages with VLDL (150  $\mu\text{g}/\text{ml}$ ) for 24 h to achieve similar TG loading as observed in  $\text{Atgl}^{-/-}$  macrophages (Fig. 5A). In accordance with the findings in  $\text{Atgl}^{-/-}$  macrophages, we found an increased number of annexin V/PI-stained cells upon incubation of WT macrophages with VLDL (Fig. 5B). Quantification of the stained cells revealed that VLDL loading increased the number of annexin V-positive cells (indicative of early apoptosis) and the number of annexin V/PI-positive cells (late apoptosis) (Fig. 5C). Similar to  $\text{Atgl}^{-/-}$  macrophages, caspase 3/7 activity was increased 4.3-fold in VLDL-loaded compared with untreated macrophages (Fig. 5D). The levels of Bcl-XL and Mcl-1 mRNA were reduced by 64 and 45%, respectively, in VLDL-treated macrophages (Fig. 5E). Additionally, we observed cleaved caspase 3 and PARP in WT cells after loading with VLDL (Fig. 5F). Bax expression was increased 1.8-fold, and cytosolic cytochrome  $c$ , which was undetectable in untreated WT macrophages, was induced (Fig. 5G). Accordingly, we found decreased protein levels of antiapoptotic Bcl-2. These phenotypes are highly similar to  $\text{Atgl}^{-/-}$  macrophages and clearly confirm increased TG concentrations as potent inducers of apoptosis.

**VLDL Loading Results in Mitochondrial Dysfunction of WT Macrophages**—Similar to what we observed in  $\text{Atgl}^{-/-}$  macrophages, VLDL loading of WT macrophages revealed a  $13 \pm 3\%$  decreased red/green fluorescence ratio in the JC-1 assay compared with unloaded macrophages, indicative of a reduced membrane potential. Fluorescence and electron micrographs of VLDL-loaded WT macrophages showed that the mitochondria exhibit features of fragmentation (Fig. 6A), very similar to the structure of mitochondria in  $\text{Atgl}^{-/-}$  macrophages (Fig. 3C). mRNA levels of NADH:ubiquinone oxidoreductase (complex I) were reduced by 44% in VLDL-loaded WT cells compared with untreated macrophages (Fig. 6B), whereas Nox1 mRNA levels were increased 10.8-fold. VLDL loading also substantially increased ROS production in WT cells by 10-fold (Fig. 6C).

Similarly to  $\text{Atgl}^{-/-}$  macrophages, basal respiration was strongly reduced by 71% upon VLDL loading compared with untreated WT macrophages (Fig. 6D). The maximal  $\text{O}_2$  consumption after FCCP treatment was also reduced in VLDL-loaded macrophages, yielding a 71% decreased spare respira-

**FIGURE 3. Activation of mitochondrial apoptosis in  $\text{Atgl}^{-/-}$  macrophages.** WT,  $\text{Atgl}^{+/+}$ , and  $\text{Atgl}^{-/-}$  macrophages were cultivated in DMEM, 10% LPDS or incubated with 100  $\mu\text{g}/\text{ml}$  acLDL (24 h) plus ACAT inhibitor 58035 (10  $\mu\text{g}/\text{ml}$ ) for the last 12 h, resembling FC loading. A, total RNA was isolated from WT,  $\text{Atgl}^{+/+}$ , and  $\text{Atgl}^{-/-}$  macrophages, and Bcl-XL and Mcl-1 mRNA levels, including normalization to HPRT, were determined by real-time PCR. Data are expressed as means ( $n = 6$ ) of two independent experiments  $\pm$  S.E. (error bars). \*\*\*,  $p \leq 0.001$ ; ##,  $p \leq 0.01$ ; ###,  $p \leq 0.001$ . B, cells were lysed and subjected to cell fractionation. Cytosolic fractions were separated by SDS-PAGE and analyzed for Bcl-2, Bax, and cytochrome  $c$  expression by Western blotting. Expression of the respective proteins from three blots was quantified relative to  $\beta$ -actin expression. Data are presented as means  $\pm$  S.E. C, cells were stained with MitoTracker Green (0.5  $\mu\text{M}$ ) and Nile Red (2.5  $\mu\text{g}/\text{ml}$ ) for 5 min. Representative confocal laser-scanning microscopy images are shown. Scale bars, 5  $\mu\text{m}$ . Shown are representative electron micrographs (TEM) of mitochondria (indicated by arrows) in WT,  $\text{Atgl}^{+/+}$ , and  $\text{Atgl}^{-/-}$  macrophages. LD, lipid droplet. Scale bars, 0.5  $\mu\text{m}$ . D, NADH:ubiquinone oxidoreductase (complex I) and NADPH oxidase activator (Nox1) mRNA levels, including normalization to HPRT, were determined in WT and  $\text{Atgl}^{-/-}$  macrophages by real-time PCR. Data are expressed as mean values ( $n = 6$ )  $\pm$  S.E. \*\*\*,  $p \leq 0.001$ ; ###,  $p \leq 0.001$ . E, WT,  $\text{Atgl}^{+/+}$ , and  $\text{Atgl}^{-/-}$  macrophages were stained with 50  $\mu\text{M}$  DCFDA for 10 min. Intracellular ROS production in macrophages was determined by the conversion of DCFDA to fluorescent DCF (excitation, 488 nm; emission, 535 nm) measured in a FlexStation<sup>TM</sup> II device (Molecular Devices). Data are expressed as mean values ( $n = 3$ )  $\pm$  S.E. \*\*\*,  $p \leq 0.001$ ; ##,  $p \leq 0.01$ . F, basal respiration was determined in untreated WT and  $\text{Atgl}^{-/-}$  macrophages. ATP synthase was inhibited with 2  $\mu\text{g}/\text{ml}$  oligomycin, followed by uncoupling of the respiratory chain from oxidative phosphorylation by a stepwise titration with FCCP to achieve maximal  $\text{O}_2$  consumption. Data are expressed as means of cell preparations from 4–10 animals performed in two independent experiments  $\pm$  S.E. \*,  $p < 0.05$ . All statistical significances were determined by ANOVA followed by Bonferroni's *post hoc* test.

## Macrophage Apoptosis by Intracellular TG Accumulation

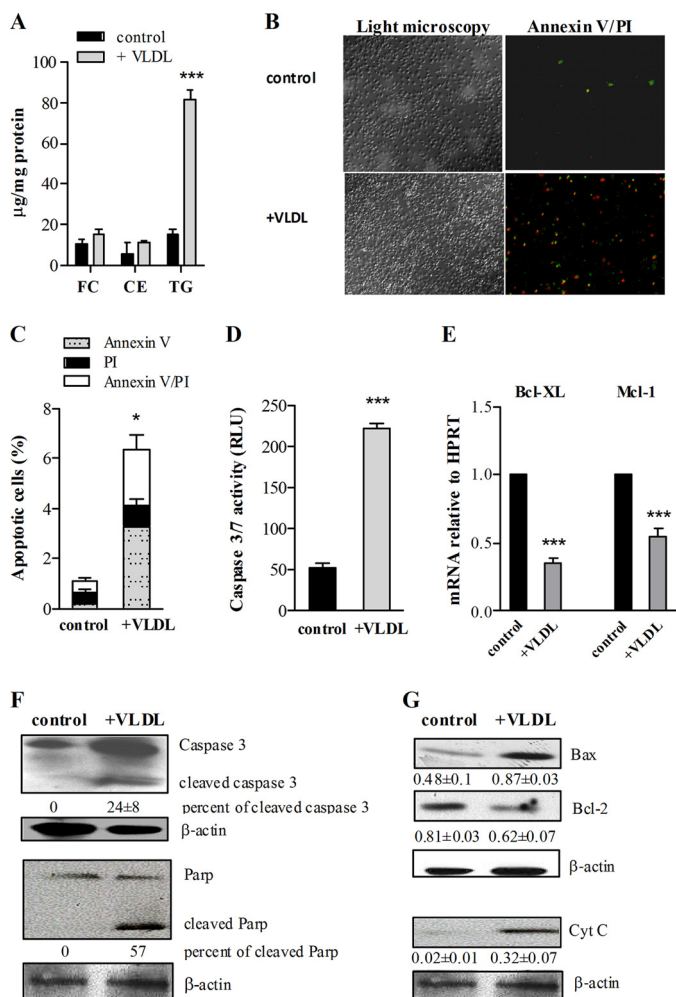


**FIGURE 5. Induction of apoptosis in VLDL-loaded WT macrophages.** WT macrophages were cultivated in DMEM, 10% LPDS in the absence (control) or presence of VLDL (150  $\mu\text{g}/\text{ml}$ , 24 h). **A**, intracellular FC, CE, and TG concentrations were measured enzymatically. \*\*\*,  $p \leq 0.001$ . **B**, apoptotic cells were determined by FITC-conjugated annexin V (green) and PI (red) co-staining, and images were taken by fluorescence microscopy. Original magnification,  $\times 10$ . **C**, quantification of fluorescence signals from three fields of cells ( $\sim 650$  cells/field) for each condition is shown. Data are expressed as the percentage of cells stained with annexin V and PI (means  $\pm$  S.E. (error bars) from three independent experiments performed in duplicate). \*,  $p < 0.05$ . **D**, combined caspase 3 and 7 activities were measured in cell lysates from untreated and VLDL-loaded WT macrophages. Data are presented as mean values ( $n = 4$ )  $\pm$  S.E. \*\*\*,  $p \leq 0.001$ . **E**, total RNA was isolated from untreated and VLDL-loaded WT macrophages, and Bcl-XL and Mcl-1 mRNA levels, including normalization to HPRT, were determined by real-time PCR. Data are expressed as means  $\pm$  S.E. of three independent experiments performed in triplicate. \*\*\*,  $p \leq 0.001$ . **F** and **G**, cell extracts (40  $\mu\text{g}$  of protein/lane) were resolved by SDS-PAGE and protein expression of caspase 3 and PARP (**F**) and Bax, Bcl-2, and cytochrome *c* (Cyt C) (**G**) was analyzed by Western blotting. Expression of the respective proteins was quantified relative to  $\beta$ -actin expression. Data are presented as means of three independent experiments  $\pm$  S.E. All statistical significances were determined by Student's *t* test.

tory capacity in VLDL-loaded compared with untreated WT macrophages (Fig. 6D).

## DISCUSSION

Apoptotic cell death is a hallmark feature of late atherosclerotic lesions (3, 25). Apoptosis results from loading macrophages with FC but not with CE. In particular, macrophage apoptosis occurs when safety mechanisms to prevent excess FC accumulation fail (3, 7, 8, 26). Approximately 9–15% apoptotic

cells were observed *in vitro* after loading primary macrophages with FC (7, 9, 10). In the present study, we investigated the effect of TG accumulation on macrophage cell death by using two different models: (i) *Atgl*<sup>-/-</sup> macrophages with defective TG hydrolysis, which accumulate cytosolic LDs even in the absence of exogenous stimuli and (ii) WT macrophages loaded with VLDL to mimic the increased intracellular TG concentrations observed in *Atgl*<sup>-/-</sup> macrophages. As a positive control, we used the established model of WT macrophages loaded with FC.

Macrophages lacking only one functional allele of ATGL show 1.7-fold increased intracellular TG concentrations compared with WT macrophages but no significant increase in annexin V-positive cells. In contrast, macrophages lacking ATGL, which exhibit 4.3-fold higher TG levels compared with *Atgl*<sup>+/-</sup> macrophages, display externalization of phosphatidylserine, a hallmark of an apoptotic event. We focused on the mitochondrial apoptosis pathway, due to its importance in cellular death events (27, 28) and in FC-triggered apoptosis (8). Indeed, we observed spontaneous caspase 3 and PARP cleavage in untreated *Atgl*<sup>-/-</sup> but not in *Atgl*<sup>+/-</sup> or WT macrophages. To achieve a similar effect in WT macrophages, the cells had to be exogenously triggered with FC or VLDL. The proteolytic processing of the inactive procaspase 3 to the active caspase 3 represents an essential step in the mitochondria-dependent apoptotic cascade (7). Consistently, cytochrome *c* was present in the cytosol of *Atgl*<sup>-/-</sup> macrophages. PARP cleavage is required for the translocation of AIF from the mitochondria to the nucleus (29, 30). In *Atgl*<sup>-/-</sup> macrophages, we observed AIF localization in the nucleus. Both AIF and cytochrome *c* are important for cell viability when they are located in mitochondria, but when either factor is released, death programs are activated. To investigate whether an additional stimulus potentiates apoptotic cell death of *Atgl*<sup>-/-</sup> macrophages, we also included FC-loaded *Atgl*<sup>-/-</sup> macrophages in some experiments. Because apoptotic features were comparable between untreated and FC-loaded *Atgl*<sup>-/-</sup> macrophages, we hypothesize that programmed cell death by ATGL deficiency and FC loading converge on the same pathway.

Most of the apoptotic features described above were also observed in VLDL-loaded WT cells, suggesting that TG accumulation in macrophages triggers apoptotic cell death. In *Atgl*<sup>-/-</sup> macrophages, spontaneous induction of apoptosis might also be due to energy deprivation as a consequence of defective lipolysis. We have previously reported that FFAs taken up by macrophages first have to be esterified to TG (and CE) for the subsequent usage as energy substrate by ATGL hydrolysis (22). We observed reduced ATP and increased ADP/ATP ratios in *Atgl*<sup>-/-</sup> macrophages. In *Atgl*<sup>+/-</sup> macrophages, ATP concentrations were comparable with those of WT macrophages (supplemental Fig. S6), indicating that one functional allele of ATGL fulfills the needs of the cells and is enough to normalize the impaired energy metabolism observed in *Atgl*<sup>-/-</sup> macrophages with decreased total acyl-CoA and acylcarnitine concentrations (22). Decreased acetyl-CoA levels indicated defective  $\beta$ -oxidation and less NADH and FADH<sub>2</sub> available for oxidative phosphorylation to drive ATP synthesis in *Atgl*<sup>-/-</sup> macrophages. In VLDL-loaded WT macrophages,

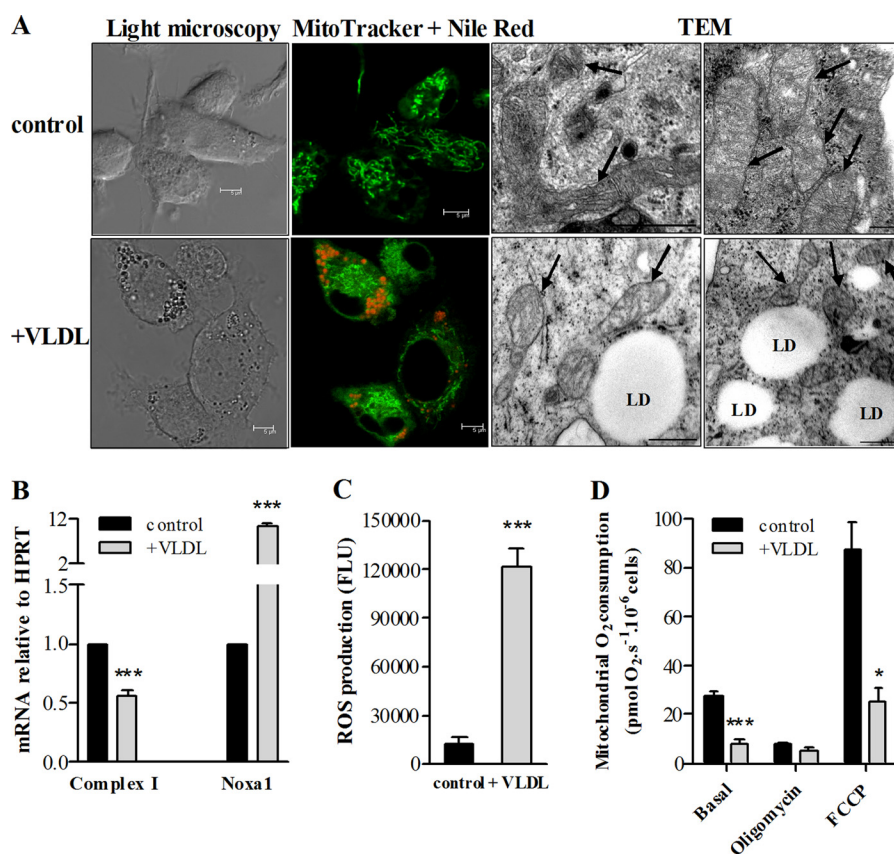


**FIGURE 6. Mitochondrial dysfunction in VLDL-loaded WT macrophages.** WT macrophages were cultivated in DMEM, 10% LPDS in the absence (control) or presence of VLDL (150  $\mu\text{g}/\text{ml}$ , 24 h). *A*, cells were stained with MitoTracker Green (0.5  $\mu\text{M}$ ) and Nile Red (2.5  $\mu\text{g}/\text{ml}$ ) for 5 min. Representative confocal laser-scanning microscopy images are shown. Scale bars, 5  $\mu\text{m}$ . Representative electron micrographs (TEM) of mitochondria (indicated by arrows) in untreated (control) and VLDL-loaded WT macrophages are shown. Scale bars, 0.5  $\mu\text{m}$ . *B*, NADH:ubiquinone oxidoreductase (complex I) and NADPH oxidase activator (Noxa1) mRNA levels, including normalization to HPRT, were determined by real-time PCR. Data are expressed as mean values ( $n = 3$ ) performed in triplicate  $\pm$  S.E. (error bars). \*\*\*,  $p \leq 0.001$ . *C*, cells were stained with 50  $\mu\text{M}$  DCFDA for 10 min. Intracellular ROS production was determined by the conversion of DCFDA to fluorescent DCF in a FlexStation™ II device. \*\*\*,  $p \leq 0.001$ . *D*, oxygen consumption in mitochondria from untreated and VLDL-loaded WT macrophages. Basal respiration, oxygen consumption after ATP synthase inhibition with 2  $\mu\text{g}/\text{ml}$  oligomycin, and maximal  $\text{O}_2$  consumption by uncoupling of the respiratory chain from oxidative phosphorylation with FCCP were determined. Data are expressed as means ( $n = 6-10$ )  $\pm$  S.E. \*,  $p < 0.05$ ; \*\*\*,  $p \leq 0.001$ . All statistical significances were determined by Student's *t* test.

however, lipolysis is intact, and the TG accumulation itself probably triggers the apoptotic process.

Release of cytochrome *c* is mostly associated with a permanent loss of  $\Delta\Psi_m$  (31); however,  $\Delta\Psi_m$  was only marginally reduced in *Atgl*<sup>-/-</sup> macrophages and VLDL-loaded WT cells. The release of cytochrome *c* has also been reported for cells whose mitochondria have an apparently normal or even increased  $\Delta\Psi_m$  (28, 32, 33). Also partial disruption of the  $\Delta\Psi_m$  by genetic or metabolic stress causes elevated cytoplasmic  $\text{Ca}^{2+}$  as a consequence of the inability of mitochondria to participate in  $\text{Ca}^{2+}$  uptake (34, 35). During the process of apoptosis, AIF needs to be cleaved by  $\text{Ca}^{2+}$ -dependent calpain, for which elevation of intracellular  $\text{Ca}^{2+}$  is a prerequisite (36). We therefore propose that increased basal cytosolic  $\text{Ca}^{2+}$  levels in *Atgl*<sup>-/-</sup> macrophages might (at least in part) be responsible for AIF localization in the nucleus, contributing to apoptotic cell death. In addition, proapoptotic Bax was increased, whereas antiapoptotic Bcl-XL, Mcl-1, and Bcl-2 were decreased in *Atgl*<sup>-/-</sup> and VLDL-loaded WT macrophages, resulting in fragmented mitochondria and reduced  $\text{O}_2$  consumption. Fragmented mitochondria are defining features of apoptosis. Several mitochondria in TG-rich macrophages are clustered around LDs and

have aberrant cristae, providing evidence of considerable mitochondrial dysfunction. Impaired mitochondria generate ROS, which are capable of acting as second messengers that mediate multiple cellular responses, including apoptosis. Consistently, ROS production was increased in *Atgl*<sup>-/-</sup> macrophages and VLDL-loaded WT cells.

One important issue arising from our study is the potential physiological effect of intracellular TG accumulation in macrophages on atherosclerotic lesion formation. Apoptotic cell death was detected in atherosclerotic plaques, with increasing frequency as the plaque develops (37). However, controversies exist about the implications of macrophage apoptosis for early and late atherosclerotic lesion development (38–40). In accordance with the data presented in the present study, we observed increased intraplaque apoptosis in *Ldlr*<sup>-/-</sup> (low density lipoprotein receptor) mice transplanted with *Atgl*<sup>-/-</sup> bone marrow compared with *Ldlr*<sup>-/-</sup> mice transplanted with bone marrow from WT animals (41). *Ldlr*<sup>-/-</sup> mice lacking ATGL in macrophages exhibited a reduced number of white blood cells, similar to what we observed in *Atgl*<sup>-/-</sup> compared with WT mice (supplemental Fig. S5). Notably, macrophage count and plaque development were markedly reduced in sections from

## Macrophage Apoptosis by Intracellular TG Accumulation

*Ldlr*<sup>-/-</sup> mice lacking ATGL, arguing for an attenuation of atherosclerosis by macrophage apoptosis (41).

In summary, data presented in this study demonstrate that ATGL plays an important role in the survival of macrophages. TG accumulation and energy deprivation in *Atgl*<sup>-/-</sup> macrophages and TG accumulation in VLDL-loaded WT macrophages result in apoptosis involving mitochondrial dysfunction and activation of the mitochondrial apoptosis pathway. Our findings provide conclusive evidence that high intracellular TG concentrations exert lipotoxic effects in macrophages and support a novel principle for lipotoxic cell death, including implications for the pathogenesis of atherosclerosis.

*Acknowledgments*—We thank S. Povoden and A. Ibovnik for excellent technical assistance and A. Hermann and I. Hindler for mouse care.

### REFERENCES

- Guo, Y., Cordes, K. R., Farese, R. V., Jr., and Walther, T. C. (2009) *J. Cell Sci.* **122**, 749–752
- Brown, M. S., Ho, Y. K., and Goldstein, J. L. (1980) *J. Biol. Chem.* **255**, 9344–9352
- Tabas, I. (2002) *J. Clin. Invest.* **110**, 905–911
- Zhang, K., and Kaufman, R. J. (2003) *Nat. Cell Biol.* **5**, 769–770
- Warner, G. J., Stoudt, G., Bamberger, M., Johnson, W. J., and Rothblat, G. H. (1995) *J. Biol. Chem.* **270**, 5772–5778
- Ho, Y. K., Brown, M. S., and Goldstein, J. L. (1980) *J. Lipid Res.* **21**, 391–398
- Yao, P. M., and Tabas, I. (2000) *J. Biol. Chem.* **275**, 23807–23813
- Yao, P. M., and Tabas, I. (2001) *J. Biol. Chem.* **276**, 42468–42476
- Devries-Seimon, T., Li, Y., Yao, P. M., Stone, E., Wang, Y., Davis, R. J., Flavell, R., and Tabas, I. (2005) *J. Cell Biol.* **171**, 61–73
- Feng, B., Yao, P. M., Li, Y., Devlin, C. M., Zhang, D., Harding, H. P., Sweeney, M., Rong, J. X., Kuriakose, G., Fisher, E. A., Marks, A. R., Ron, D., and Tabas, I. (2003) *Nat. Cell Biol.* **5**, 781–792
- Timmins, J. M., Ozcan, L., Seimon, T. A., Li, G., Malagelada, C., Backs, J., Backs, T., Bassel-Duby, R., Olson, E. N., Anderson, M. E., and Tabas, I. (2009) *J. Clin. Invest.* **119**, 2925–2941
- Ullery-Ricewick, J. C., Cox, B. E., Griffin, E. E., and Jerome, W. G. (2009) *J. Lipid Res.* **50**, 2014–2026
- Zimmermann, R., Strauss, J. G., Haemmerle, G., Schoiswohl, G., Birner-Gruenberger, R., Riederer, M., Lass, A., Neuberger, G., Eisenhaber, F., Hermetter, A., and Zechner, R. (2004) *Science* **306**, 1383–1386
- Jenkins, C. M., Mancuso, D. J., Yan, W., Sims, H. F., Gibson, B., and Gross, R. W. (2004) *J. Biol. Chem.* **279**, 48968–48975
- Villena, J. A., Roy, S., Sarkadi-Nagy, E., Kim, K. H., and Sul, H. S. (2004) *J. Biol. Chem.* **279**, 47066–47075
- Haemmerle, G., Zimmermann, R., Hayn, M., Theussl, C., Waeg, G., Wagner, E., Sattler, W., Magin, T. M., Wagner, E. F., and Zechner, R. (2002) *J. Biol. Chem.* **277**, 4806–4815
- Haemmerle, G., Lass, A., Zimmermann, R., Gorkiewicz, G., Meyer, C., Rozman, J., Heldmaier, G., Maier, R., Theussl, C., Eder, S., Kratky, D., Wagner, E. F., Klingenspor, M., Hoefler, G., and Zechner, R. (2006) *Science* **312**, 734–737
- Fischer, J., Lefèvre, C., Morava, E., Mussini, J. M., Laforêt, P., Negre-Salvayre, A., Lathrop, M., and Salvayre, R. (2007) *Nat. Genet.* **39**, 28–30
- Hirano, K., Ikeda, Y., Zaima, N., Sakata, Y., and Matsumiya, G. (2008) *N. Engl. J. Med.* **359**, 2396–2398
- Akiyama, M., Sakai, K., Ogawa, M., McMillan, J. R., Sawamura, D., and Shimizu, H. (2007) *Muscle Nerve* **36**, 856–859
- Kobayashi, K., Inoguchi, T., Maeda, Y., Nakashima, N., Kuwano, A., Eto, E., Ueno, N., Sasaki, S., Sawada, F., Fujii, M., Matoba, Y., Sumiyoshi, S., Kawate, H., and Takayanagi, R. (2008) *J. Clin. Endocrinol. Metab.* **93**, 2877–2884
- Chandak, P. G., Radovic, B., Aflaki, E., Kolb, D., Buchebner, M., Fröhlich, E., Magnes, C., Sinner, F., Haemmerle, G., Zechner, R., Tabas, I., Levak-Frank, S., and Kratky, D. (2010) *J. Biol. Chem.* **285**, 20192–20201
- Basu, S. K., Goldstein, J. L., Anderson, G. W., and Brown, M. S. (1976) *Proc. Natl. Acad. Sci. U.S.A.* **73**, 3178–3182
- Karlsson, M., Kurz, T., Brunk, U. T., Nilsson, S. E., and Frennesson, C. I. (2010) *Biochem. J.* **428**, 183–190
- Li, Y., Schwabe, R. F., DeVries-Seimon, T., Yao, P. M., Gerbod-Giannone, M. C., Tall, A. R., Davis, R. J., Flavell, R., Brenner, D. A., and Tabas, I. (2005) *J. Biol. Chem.* **280**, 21763–21772
- Kellner-Weibel, G., Jerome, W. G., Small, D. M., Warner, G. J., Stoltenberg, J. K., Kearney, M. A., Corjay, M. H., Phillips, M. C., and Rothblat, G. H. (1998) *Arterioscler. Thromb. Vasc. Biol.* **18**, 423–431
- Kroemer, G., and Reed, J. C. (2000) *Nat. Med.* **6**, 513–519
- Green, D. R., and Reed, J. C. (1998) *Science* **281**, 1309–1312
- Yu, S. W., Wang, H., Poitras, M. F., Coombs, C., Bowers, W. J., Federoff, H. J., Poirier, G. G., Dawson, T. M., and Dawson, V. L. (2002) *Science* **297**, 259–263
- Susin, S. A., Lorenzo, H. K., Zamzami, N., Marzo, I., Snow, B. E., Brothers, G. M., Mangion, J., Jacotot, E., Costantini, P., Loeffler, M., Larochette, N., Goodlett, D. R., Abersold, R., Siderovski, D. P., Penninger, J. M., and Kroemer, G. (1999) *Nature* **397**, 441–446
- Heiskanen, K. M., Bhat, M. B., Wang, H. W., Ma, J., and Nieminen, A. L. (1999) *J. Biol. Chem.* **274**, 5654–5658
- Szalai, G., Krishnamurthy, R., and Hajnóczky, G. (1999) *EMBO J.* **18**, 6349–6361
- Vander Heiden, M. G., Chandel, N. S., Schumacker, P. T., and Thompson, C. B. (1999) *Mol. Cell* **3**, 159–167
- Amuthan, G., Biswas, G., Ananadatheerthavarada, H. K., Vijayarathay, C., Shephard, H. M., and Avadhani, N. G. (2002) *Oncogene* **21**, 7839–7849
- Arnould, T., Vankoningsloo, S., Renard, P., Houbion, A., Ninane, N., Demazy, C., Remacle, J., and Raes, M. (2002) *EMBO J.* **21**, 53–63
- Norberg, E., Gogvadze, V., Ott, M., Horn, M., Uhlén, P., Orrenius, S., and Zhivotovsky, B. (2008) *Cell Death Differ.* **15**, 1857–1864
- Lutgens, E., de Muinck, E. D., Kitslaar, P. J., Tordoir, J. H., Wellens, H. J., and Daemen, M. J. (1999) *Cardiovasc. Res.* **41**, 473–479
- Thorp, E., Cui, D., Schrijvers, D. M., Kuriakose, G., and Tabas, I. (2008) *Arterioscler. Thromb. Vasc. Biol.* **28**, 1421–1428
- Thorp, E., Li, Y., Bao, L., Yao, P. M., Kuriakose, G., Rong, J., Fisher, E. A., and Tabas, I. (2009) *Arterioscler. Thromb. Vasc. Biol.* **29**, 169–172
- Liu, J., Thewke, D. P., Su, Y. R., Linton, M. F., Fazio, S., and Sinensky, M. S. (2005) *Arterioscler. Thromb. Vasc. Biol.* **25**, 174–179
- Lammers, B., Chandak, P. G., Aflaki, E., Van Puijvelde, G. H., Radovic, B., Hildebrand, R. B., Meurs, I., Out, R., Kuiper, J., Van Berkel, T. J., Kolb, D., Haemmerle, G., Zechner, R., Levak-Frank, S., Van Eck, M., and Kratky, D. (2011) *Arterioscler. Thromb. Vasc. Biol.* **31**, 67–73